

Statistical lensing by galactic disks

A. W. Blain,¹ Ole Möller¹ and Ariyeh H. Maller²

¹ Cavendish Laboratory, Madingley Road, Cambridge, CB3 0HE.

² Physics Department, University of California, Santa Cruz, Santa Cruz, CA 95064, USA.

2 December 2024

ABSTRACT

The high-magnification gravitational lensing cross section of a galaxy is enhanced significantly if a baryonic disk is embedded in its dark matter halo. We investigate the effects of a population of such disks on the probability of detecting strongly lensed images of distant galaxies and quasars. The optical depth to lensing is always more than doubled. The effects are particularly significant at magnifications greater than about 50, for which the optical depth typically increases by a factor greater than 5. If either the fraction of disks or the typical disk-to-halo mass ratio increases with redshift, then the optical depth is expected to be increased even further. Obscuration by dust in the lensing disk is expected to counteract the associated enhanced magnification bias for surveys in the optical waveband, but not in the radio and millimetre/submillimetre wavebands. The presence of galactic disks should hence lead to a significant increase in the number of lensed galaxies and quasars detected in both radio- and millimetre/submillimetre-selected surveys. An increase by a factor of about 3 is expected, enhancing the strong case for millimetre/submillimetre-wave lens surveys using the next generation of ground-based telescopes and the *FIRST* and *Planck Surveyor* space missions.

Key words: galaxies: evolution – galaxies: fundamental parameters – cosmology: theory – gravitational lensing – radio continuum: galaxies

1 INTRODUCTION

There has been much recent interest in the effects of galactic disks on the lensing cross sections of galaxies (Bartelmann & Loeb 1998; Keeton & Kochanek 1998; Koopmans, De Bruyn & Jackson 1998; Maller, Flores & Primack 1997; Möller & Blain 1998; Wang & Turner 1997). A gravitationally-dominant baryonic disk in the core of a dark matter halo, edge-on to the line of sight to a distant source, can significantly increase the mass surface density, and thus the lensing efficiency.

The image geometry produced by an individual lens can be modified significantly by the presence of an edge-on or almost edge-on disk; however, the cross section to multiple imaging is only increased by a factor of about 50 per cent when averaged over all disk inclinations. In contrast, the cross section to magnifications greater than 10 is expected to be increased by a factor of a few after the same averaging process (Möller & Blain 1998). Hence, depending on the abundance and form of evolution of disks in dark matter halos, the strong lensing optical depth at moderate and large redshifts could be increased very significantly. Bartelmann & Loeb (1998) have also recently discussed this effect. They note that it will probably not be possible to exploit any enhanced magnification in the optical waveband because the

flux densities of the lensed images will be attenuated by dust associated with the disk. For the same reason, Maller et al. (1997) did not consider the effect of disk lensing on the magnifications of multiple images because of possible differential extinction between the images.

Dust extinction is important in the optical waveband; however, a dusty lensing disk is optically thin in the radio and millimetre/submillimetre wavebands. Indeed, because of *K*-correction effects (Blain & Longair 1993), a lensing object is often expected to be fainter than the lensed images in the submillimetre waveband (Blain 1997a, 1998b). Hence, any enhanced magnification bias due to the effects of disks would be easy to detect in these wavebands. Existing radio lens surveys, such as the CLASS survey (Browne et al. 1997), appear to show an overabundance of lens candidates that can be identified as highly inclined disks. The potential importance of submillimetre-wave lens surveys has been discussed for lensing by both clusters (Blain 1997a, 1998a) and galaxies (Blain 1996, 1997b, 1998b,c). Submillimetre-wave lensing by clusters has now been demonstrated to be a very useful phenomenon (Smail, Ivison & Blain 1997). The most striking feature of submillimetre-wave galaxy lens surveys is that the fraction of strongly lensed galaxies detected in a carefully selected sample can exceed 5 per cent (Blain 1996, 1998b).

In Section 2 we discuss the statistical features of lensing by galaxies containing a disk, using techniques and models of lensing by disk galaxies developed by Möller (1996), Maller et al. (1997) and Möller & Blain (1998), and the statistical lensing formalism (Peacock 1982; Pei 1995) applied in the submillimetre waveband by Blain (1996). In Section 3 we predict the effects of a potentially evolving population of disks (Lilly et al. 1998; Mo, Mao & White 1998; Mao, Mo & White 1998; Marzke et al. 1998) on the lensing cross sections. In Section 4 we estimate the surface density of strongly lensed galaxies and quasars in the light of recent submillimetre-wave observations by Smail et al. (1997) using the new SCUBA camera at the James Clerk Maxwell Telescope (Holland et al. 1999); see Smail et al. (1998, 1999, in preparation), Ivison et al. (1998), Blain, Ivison & Smail (1998a), Blain et al. (1998b, 1999, submitted) and Frayer et al. (1998) for a discussion of the latest results. In Section 5 the prospects for detecting such images in future surveys using forthcoming ground-based and space-borne instruments are discussed.

The values of cosmological parameters have a significant effect on the properties of galaxy–galaxy submillimetre-wave lensing (Blain 1998a). Unless otherwise stated, we assume an Einstein–de Sitter world model with Hubble’s constant $H_0 = 60 \text{ km s}^{-1} \text{ Mpc}^{-1}$, in accordance with the models presented by Maller et al. (1997) and Möller & Blain (1998). Note that the abundance of submillimetre-wave lensed galaxies predicted in an Einstein–de Sitter model is less than that expected in a model with a smaller density parameter (Blain 1998a).

2 THE STRONG LENSING OPTICAL DEPTH

2.1 Basic formalism

Millimetre/submillimetre-wave source counts of lensed images were predicted by Blain (1996), using formalism developed by Peacock (1982) and Pei (1995) to estimate the optical depth to strong lensing due to galaxies. In this formalism the probability that a source at redshift z is lensed by a magnification between μ and $\mu + d\mu$ is $F(\mu, z)$. This function is obtained by integrating the cross sections of individual lenses to magnifications greater than μ , $\sigma_\mu(M, z)$ in the plane of the lens, both along the line of sight to z and over the mass function of lenses N , and then differentiating with respect to μ ,

$$F = -\frac{d}{d\mu} \int_0^z \int_0^\infty \sigma_\mu(M, z')(1+z')^2 dN(M) \frac{dr}{dz'} dz'. \quad (1)$$

r is the comoving radial distance element. The number and flux density conservation conditions,

$$\int_0^\infty F(\mu, z) d\mu = \int_0^\infty \mu F(\mu, z) d\mu = 1, \quad (2)$$

must be satisfied. If the intrinsic luminosity function of galaxies $\Phi(L, z)$ is known, then the source count of unlensed galaxies,

$$N(S_\nu) = \frac{1}{4\pi} \int_0^{z_0} \int_{L_{\min}(S_\nu, z)}^\infty \Phi(L, z) dL \frac{D(0, z)^2}{(1+z)^2} \frac{dr}{dz} dz. \quad (3)$$

L_{\min} is the luminosity of a source at a redshift z that produces a flux density S_ν . z_0 is the maximum redshift of the

source population. $D(z_a, z_b)$ is the angular diameter distance between redshifts z_a and z_b . The count of lensed galaxies can be determined using equation (3), if Φ is replaced by an effective luminosity function,

$$\Phi'(L, z) = \int_0^{\mu_{\max}(z)} \frac{F(\mu, z)}{\mu} \Phi\left(\frac{L}{\mu}, z\right) d\mu, \quad (4)$$

corrected to include the effects of lensing. μ_{\max} , the maximum magnification, is determined by the intrinsic size of the source and the geometry of the lens configuration. In general, larger values of μ_{\max} are expected for smaller sources. $\mu_{\max}(z = 1) \simeq 25$ is expected for lensing by a singular isothermal sphere (SIS) lens if the intrinsic size of the source is 1 kpc (Peacock 1982).

2.2 Lensing by singular isothermal spheres (SISs)

The cross section to high-magnification lensing by a SIS at redshift z' for a source at redshift z , as measured in the plane of the lens,

$$\sigma_\mu^{\text{SIS}}(\mu, M_e) = 64\pi \left[\frac{G}{c^2} \frac{M_e}{R} \right]^2 \left[\frac{D(0, z') D(z', z)}{D(0, z)} \right]^2 \mu^{-2}, \quad (5)$$

(Schneider, Ehlers & Falco 1992). M_e is the mass of the lens enclosed within a radius R . The distance ratio inside the second square bracket is referred to as $D_R(z', z)$ in subsequent equations. In the case of lensing by SISs, the magnification and redshift dependences of F (equation 1) can be separated at large magnifications, yielding the strong lensing probability $F_{\text{SIS}} = a(z)\mu^{-3}$ that is applicable here. The form of F_{SIS} at all magnifications can be approximated by,

$$F_{\text{SIS}} = H\delta(\mu - \mu_0) + \begin{cases} a(z)\mu^{-3}, & \text{if } \mu_t \leq \mu \leq \mu_{\max}; \\ 0, & \text{otherwise.} \end{cases} \quad (6)$$

The first term describes the typically small magnification correction that must be applied to most sources in order to satisfy the number and flux density conservation conditions (equation 2).

The form of the function $a(z)$ depends on both the values of cosmological parameters and the form of evolution of lensing galaxies (Blain 1996, 1998a). If the distribution of lenses in mass M is described by a Press–Schechter function (Press & Schechter 1974),

$$dN(M, z) = \frac{\bar{\rho}_g}{\sqrt{\pi}} \frac{\gamma}{M^2} \left(\frac{M}{M^*} \right)^{\gamma/2} \exp \left[-\left(\frac{M}{M^*} \right)^\gamma \right] dM, \quad (7)$$

then equation (1) can be evaluated analytically. $M^*(z)$ includes all the details of the evolution of structure due to the growth of perturbations in an expanding Universe. $\gamma = 4/3$ if the primordial density fluctuations are scale independent. $\bar{\rho}_g$ is the mean smoothed density of bound objects in the Universe. M is the mass of a region of the Universe that has turned around from the Hubble flow and is in the process of collapse at a particular epoch. M is related to the mass enclosed within a radius R , M_e (equation 5) by the constant ϵ , that is,

$$M_e = \epsilon M. \quad (8)$$

M_e^* is the equivalently transformed version of M^* . This transformation allows the masses in equations (5) and (7) to

be linked in the same expression. For example, if the population of lensing galaxies consists entirely of SISs, then by evaluating equation (1),

$$a(z) = 128\sqrt{\pi}\bar{\rho}_g\epsilon \left[\frac{G}{c^2 R} \right]^2 \Gamma \left[\frac{1}{\gamma} + \frac{1}{2} \right] \times \int_0^z D_R^2(z', z) (1+z')^2 M_e^*(z') \frac{dr}{dz'} dz'. \quad (9)$$

If F_{SIS} is given by equation (6) then,

$$\Phi'_{\text{SIS}} = \frac{H}{\mu_0} \Phi \left(\frac{L}{\mu_0} \right) + a(z) \int_{\mu_t}^{\mu_{\text{max}}(z)} \frac{I(\mu)}{\mu} \Phi \left(\frac{L}{\mu} \right) d\mu, \quad (10)$$

in which $I(\mu) = \mu^{-3}$. This equation was used to derive the results for the probabilities of statistical lensing presented by Blain (1996, 1998a).

2.3 Lensing by disks

Möller & Blain (1998) recently presented the results of simulations of the high-magnification lensing cross section for an exponential disk embedded within a SIS halo. When the disk was within about 30 degrees of being edge-on to the line of sight, this cross section was found to be increased by a significant factor as compared with that for a SIS halo alone. An example of the relative magnification $\sigma_\mu/\sigma_\mu^{\text{SIS}}$ is plotted in Fig. 3(a) of Möller & Blain (1998), for a disk/halo combination well matched to that of the Milky Way. We have now extended these simulations to include a wide range of halo and disk masses, and so to investigate the statistical properties of lensing by such objects. The central surface mass density of the disk within the halo was kept constant (Mao, Mo & White 1998), while the scale length of the disk was varied in such a way that the ratio of the mass of dark matter in the SIS halo within a radius $R = 10$ kpc and the mass of the disk remained constant. The results are now parametrized to generate an analytical description of the effects of lensing by a population of disks.

2.3.1 Formalism

The relative cross section to lensing by a magnification greater than μ due to a combination of a disk and a SIS halo, as compared with a SIS halo alone, was approximated by a function of the form,

$$\frac{\sigma_\mu}{\sigma_\mu^{\text{SIS}}} = C(M_e) \begin{cases} \frac{(\beta - \alpha)\mu_*^{1+\alpha}\mu^2}{1 + \alpha + \beta + \alpha\beta} - \frac{\mu^{3+\alpha}}{1 + \alpha}, & \text{if } \mu \leq \mu_*; \\ -\frac{\mu_*^{\alpha-\beta}\mu^{3+\beta}}{1 + \beta}, & \text{otherwise,} \end{cases} \quad (11)$$

where,

$$C(M_e) = K \left[1 + \left(\frac{M_e}{M_0} \right)^\eta \right]. \quad (12)$$

Any systematic evolution of the scale length/mass of disks within dark matter halos can be incorporated by modifying the value of M_0 , defined as the mass of dark matter enclosed within 10 kpc of the core of a SIS halo, as a function of redshift.

Equation (11) has the useful property that when differentiated to obtain $d\sigma_\mu/d\mu$ – required in equation (1), the result has a simple double-power-law form,

Table 1. The values of the best-fitting parameters derived from the extended results of Möller & Blain (1998). The associated best-fitting curves are shown in Fig. 1. The best fitting values of the worst constrained parameters, β and μ_* , are related by the equation $\beta = 0.017\mu_* - 2.6$.

Parameter	Value	Parameter	Value
α	-2.85 ± 0.16	β	$-2.12^{+0.25}_{-0.14}$
η	-0.87 ± 0.06	μ_*	26^{+14}_{-8}
M_0	$(2.6 \pm 0.4) \times 10^{11} M_\odot$	K	1.7 ± 0.5
M_e^*	$2.9 \times 10^{11} M_\odot$		

$$\frac{d\sigma_\mu}{d\mu} = 64\pi \left[\frac{G}{c^2} \frac{M_e}{R} \right]^2 C(M_e) \begin{cases} \mu^\alpha, & \text{if } \mu \leq \mu_*; \\ \mu_*^{\alpha-\beta} \mu^\beta, & \text{otherwise.} \end{cases} \quad (13)$$

The parameters α , β , μ_* , K , M_0 and η were determined by fitting the function in equation (11) to the results of the numerical simulations (Möller & Blain 1998). The form of the best-fitting models, and probability contours determined by fitting to the worst-constrained pairs of parameters, β and μ_* and η and M_0 , are all shown in Fig. 1. The values of all the best-fitting parameters are listed in Table 1.

The resulting model for the cross section to strong lensing by disks within SIS halos can be used to estimate the optical depth to strong lensing F_{disk} . F_{disk} is obtained as a function of redshift by evaluating equation (1), incorporating the fraction of halos that contain a baryonic disk $f_d(z)$:

$$F_{\text{disk}} = -\frac{d}{d\mu} \int_0^z \int_0^\infty (1+z')^2 \frac{dr}{dz'} \times \left[(1-f_d)\sigma_\mu^{\text{SIS}}(M) + f_d\sigma_\mu(M) \right] dN(M) dz'. \quad (14)$$

For magnifications $\mu > \mu_t$ this can be written as,

$$F_{\text{disk}} = [a_1(z) - a_2(z)] I_n(\mu) + [a_2(z) + a_3(z)] I_d(\mu), \quad (15)$$

the sum of two magnification-dependent terms, I_n and I_d , which are modulated by redshift-dependent terms that are combinations of three functions; a_1 , a_2 and a_3 . As in equation (6), a low-magnification correction term containing H and μ_0 must be included in order to approximate the complete probability function.

I_n and I_d are associated with lensing by pure SIS halos and by disks within SIS halos respectively.

$$I_n(\mu) = \mu^{-3}, \quad (16)$$

and,

$$I_d(\mu) = \frac{K}{2} \begin{cases} \mu^\alpha, & \text{if } \mu \leq \mu_*; \\ \mu_*^{\alpha-\beta} \mu^\beta, & \text{otherwise.} \end{cases} \quad (17)$$

The a -functions (equation 15),

$$a_1(z) = \Gamma \left[\frac{1}{\gamma} + \frac{1}{2} \right] \int_0^z J(z') M_e^*(z') dz', \quad (18)$$

$$a_2(z) = \Gamma \left[\frac{1}{\gamma} + \frac{1}{2} \right] \int_0^z J(z') f_d(z') M_e^*(z') dz', \quad (19)$$

and,

$$a_3(z) = \Gamma \left[\frac{\eta+1}{\gamma} + \frac{1}{2} \right] \int_0^z J(z') \frac{M_e^*(z')^{(1+\eta)}}{M_0(z')^\eta} f_d(z') dz', \quad (20)$$

in all three of which,

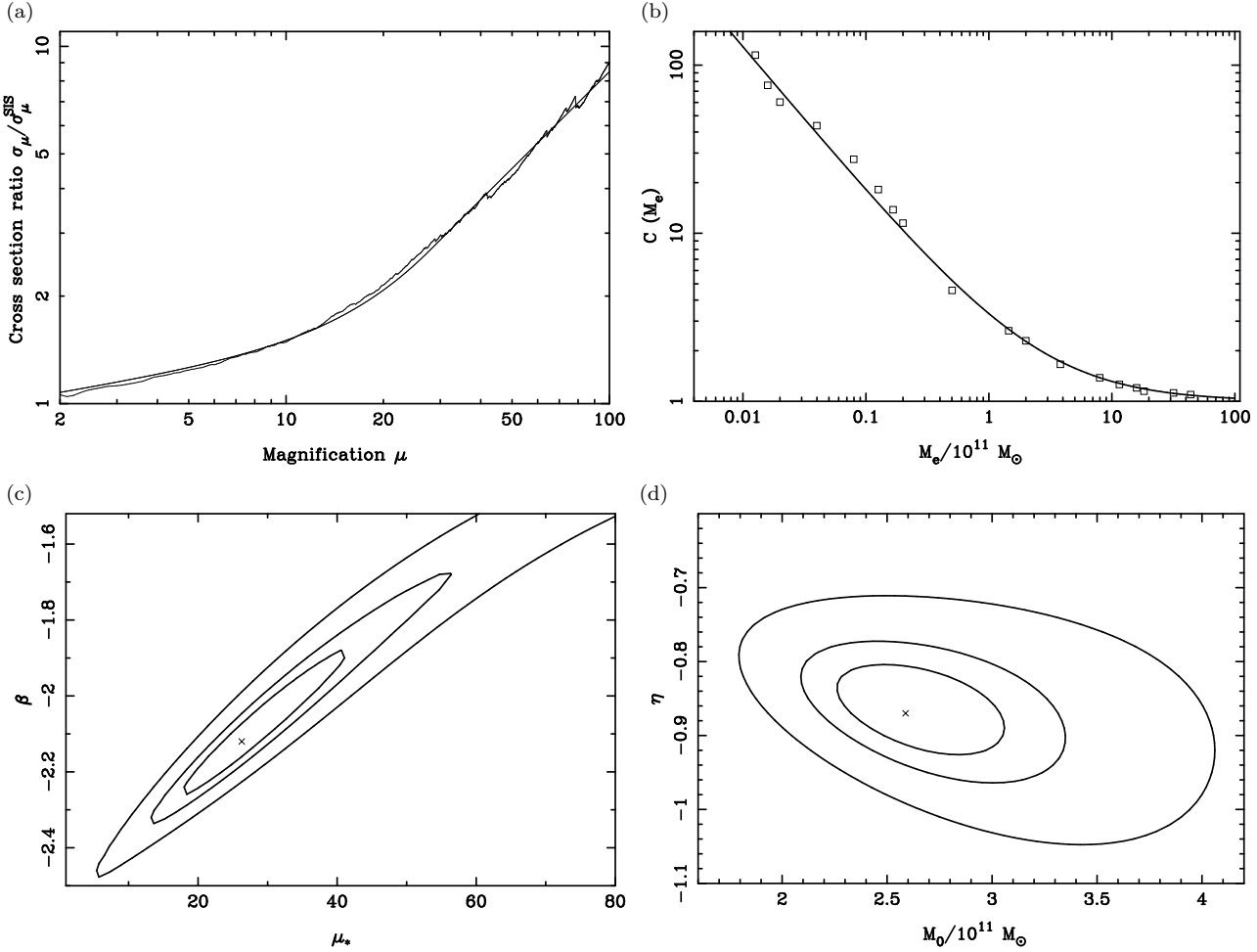


Figure 1. The best-fitting models that describe the magnification dependence of the function $\sigma_\mu/\sigma_\mu^{\text{SIS}}$ (equation 11) (a) and the mass dependence of the function $C(M_e)$ (equation 12) (b), shown by the smooth curves. The results of the simulations are shown by the jagged line in (a) and the empty squares in (b) respectively. The quality of the constraints imposed on the worst-constrained pairs of parameters in each case are shown in (c) and (d) respectively. The three contour levels correspond to likelihoods 1σ , 2σ and 3σ away from the maximum value, which is marked by a cross. The values of the best-fitting parameters are listed in Table 1.

$$J(z') = 128\sqrt{\pi}\bar{\rho}\epsilon \left[\frac{G}{c^2 R} \right]^2 D_R^2(z', z) (1+z')^2 \frac{dr}{dz'}. \quad (21)$$

Note that if disks do not evolve, then the redshift dependences of a_1 , a_2 and a_3 are identical.

The relative normalization of a_3 as compared with a_1 and a_2 depends on the ratio of the mass M_0 , derived from the results of the numerical simulations described above, and the typical mass in the Press-Schechter function M_e^* (equations 7 and 8). The value of M_e^* can be determined by using the Tully-Fisher relation (Hudson et al. 1998), an empirical power-law relation between the B -band luminosity and circular velocity of galaxies. A circular velocity $v_c \simeq 360 \text{ km s}^{-1}$ is indicated by the Tully-Fisher relation for an L^* galaxy with a B -band magnitude $M_B = -21$ at the present epoch. If L^* is assumed to be equivalent to M^* , then M_e^* can be determined by comparison with the Milky Way, for which $M_e(R < 10 \text{ kpc}) = 10^{11} M_\odot$ and $v_c \simeq 210 \text{ km s}^{-1}$. $M_e^* \simeq 2.9 \times 10^{11} M_\odot$ is expected in this case.

By combining equations (15) to (21), we can model the optical depth to strong lensing by a population of SIS dark matter halos that contain an evolving population of baryonic disks. A new effective luminosity function Φ'_{disk} can be

produced by including the general form of F_{disk} in equation (4). In order to evaluate the count of lensed sources using this function, the forms of $a_1(z)$, $a_2(z)$, $a_3(z)$, $f_d(z)$ and $M_0(z)$ are required. The redshift dependence of the a -functions in both hierarchical and non-hierarchical models, and three different world models is illustrated in Fig. 2. The form of evolution of disks, discussed by Lilly et al. (1998) and Mao, Mo & White (1998), is considered in Section 3.1.

We parametrize the fraction of halos that contain disks $f_d = f_0(1+z)^p$ and the scale length $r_s \propto (1+z)^{q/2}$. The comoving abundance of disks and the mass of the disk within a typical halo are thus expected to evolve as $M^*(z)^{-1}f_d(z)$ and $M^*(z)(1+z)^q$ respectively, if the central surface density of the disk is assumed to be independent of redshift. In an Einstein-de Sitter model, $M^* \propto (1+z)^{-1}$ would be expected due to the hierarchical evolution of bound objects.

2.3.2 Normalization of the terms in F_{disk}

The relative size of the two terms in equation (15) depends on the parameters f_0 , p , q and $\bar{\rho}\epsilon$. To clarify the dependence of the results on the form of evolution, we introduce the

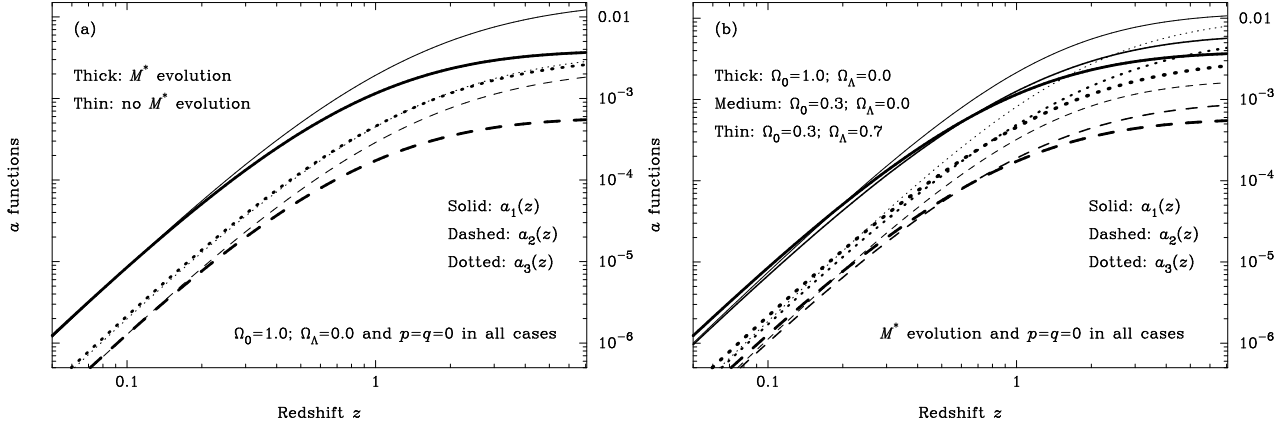


Figure 2. A comparison of the three redshift-dependent a -functions that contribute to F_{disk} (equation 15). In (a) the effects of including evolution of M^* in the Press–Schechter function are shown. a_1 and a_2 are affected in the same way, but the effect on a_3 is much less significant. In (b) M^* is assumed to evolve, and the effects of three different world models are compared: see also Blain (1998a). The functions are normalized to match the low-redshift value of $a(z)$ used in Blain (1996), with a value of $f_0 = 0.15$: see Section 3.1.

parameters τ and R_τ , the total probability of lensing by a magnification $\mu > \mu_t$, and the ratio of the probabilities of lensing by a disk as compared with lensing by a halo alone respectively.

$$\tau = [a_1 - a_2] \int_{\mu_t}^{\infty} I_n(\mu) d\mu + [a_2 + a_3] \int_{\mu_t}^{\infty} I_d(\mu) d\mu, \quad (22)$$

and,

$$R_\tau = \frac{a_2 + a_3}{a_1 - a_2} \frac{\int_{\mu_t}^{\infty} I_d(\mu) d\mu}{\int_{\mu_t}^{\infty} I_n(\mu) d\mu}. \quad (23)$$

At a low redshift z_1 , for which all three a -functions are proportional to z^3 , and for values of $\mu_t \simeq 2$ then,

$$\begin{aligned} \tau \simeq & 16\sqrt{\pi\rho\epsilon} \left[\frac{G}{c^2 R} \right]^2 (1 + f_0 T) \Gamma \left[\frac{1}{\gamma} + \frac{1}{2} \right] \times \\ & \int_0^{z_1} D_R^2(z', z) (1 + z')^2 M_e^*(z') \frac{dr}{dz'} dz', \end{aligned} \quad (24)$$

in which,

$$T = \frac{\Gamma \left(\frac{\eta+1}{\gamma} + \frac{1}{2} \right)}{\Gamma \left(\frac{1}{\gamma} + \frac{1}{2} \right)} \left(\frac{M_e^*}{M_0} \right)^\eta, \quad (25)$$

and,

$$R_\tau \simeq \frac{f_0}{1 - f_0} (1 + T). \quad (26)$$

Based on the values of parameters listed in Table 1, T is expected to take the value 1.6. If $\tau \simeq 10^{-5}$ at $z = 0.1$ (Blain 1996), then the density parameter associated with ρ_g , $\Omega_g \epsilon \simeq 8 \times 10^{-4}$. Hence, since $\Omega_g \sim 10^{-2}$, $\epsilon \sim 8 \times 10^{-2}$. This would indicate that 8 per cent of the mass of the dark matter in the SIS halo of a M^* galaxy at the present epoch was enclosed within 10 kpc of the core, equivalent to a truncation radius of 125 kpc for the SIS.

If $f_0 = 0.6$ (see Section 3.1), then $R_\tau \simeq 3.6$, and so about 80 per cent of lensing events should be due to disk galaxies, neglecting the effects of both magnification bias and evolution of the population of lenses.

By combining equations (24) to (26), the low-redshift normalization of the a -functions can be determined by com-

parison with the normalization of $a(z)$ in a disk-free model (equation 6): see Blain (1996) for a summary of the estimated form of $a(z)$. The normalization of a_1 is given by,

$$a_1(z_1) = \frac{1}{2} \tau_n(z_1) \mu_t^{-2} (1 + f_0 T), \quad (27)$$

where τ_n is the probability of lensing in a model without disks, to which the predictions in Blain (1996, 1998a, 1998c) were normalized. The other two a -functions are normalized to,

$$a_2(z_1) = f_0 a_1(z_1), \quad (28)$$

and,

$$a_3(z_1) = f_0 T a_1(z_1). \quad (29)$$

3 LENSING CROSS SECTION PREDICTIONS

3.1 The population and evolution of disks

Lilly et al. (1998) discussed the morphological properties of galaxies detected in the Canada–France Redshift Survey (CFRS). To avoid surface brightness selection effects they classified galaxies based on their appearance within $4 h^{-1}$ kpc of the core. They found no evidence for evolution in the abundance of spiral galaxies out to redshifts greater than 0.5. About 18 per cent of the galaxies with identifiable morphologies in the small-radius sample contained a disk. Based on a B -band selected local galaxy survey, unaffected by surface brightness selection effects, Marzke et al. (1998) find that about 64 per cent of local galaxies have a disk morphology. Brinchmann (1998) find that about 50 per cent of galaxies selected in the I -band are classified as containing a disk, either by eye or by machine. The fraction does not appear to depend strongly on either the redshift or the intrinsic luminosity of the galaxies. The zero-redshift abundance of disks in halos f_0 thus appears to be about 0.6.

Based on the results of theoretical and numerical work on the evolution of disks (Mo, Mao & White 1998), Mao, Mo & White (1998) argued that the results presented by Lilly et al. (1998) are consistent with a comoving abundance of

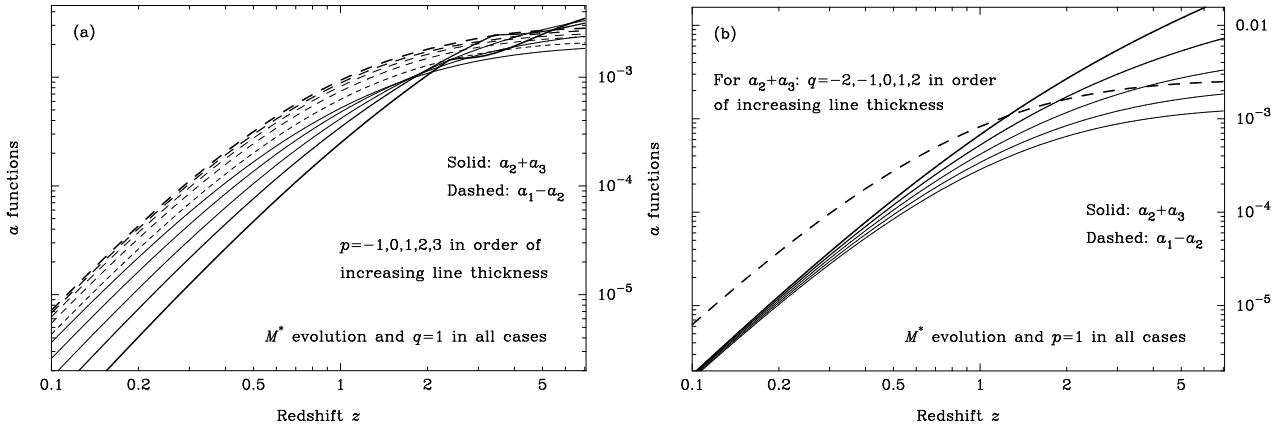


Figure 3. A comparison of the effects of disk evolution on the two redshift-dependent functions that contribute to F_{disk} (equation 15), $a_1 - a_2$ and $a_2 + a_3$. In (a) five different forms of the abundance of disks $f_d(z) = f_0(1+z)^p$ are compared, with $p = -1, 0, 1, 2$ and 3 ; the disk-to-halo mass ratio does not evolve. In each case, the value of f_0 is chosen to satisfy the constraint that the fraction of disks found in the CFRS $R_d \simeq 0.18$ (equation 30). In (b) the effects of five different forms of the evolution of $M_0 \propto (1+z)^q$ are included, with $q = -2, -1, 0, 1$ and 2 ; a value of $p = 1$ is assumed in all cases, corresponding to a value of $f_0 = 0.089$ if $R_d = 0.18$. The discontinuities in the gradients of the solid curves at high redshifts in (a) are due to f_d reaching its upper limit. Note that the strongly evolving models have values of f_0 that are much smaller than the observed zero-redshift value (Marzke et al. 1998).

disks that varies as $(1+z)^3$, and a typical scale length $r_s \propto (1+z)^{-1}$. If M^* does not evolve, then values of $p = 0$ and $q = 0$ correspond to no evolution of either the abundance or the typical scale length of disks (Lilly et al. 1998); if M^* does evolve, then values of $p = -1$ and $q = 1$ would be required. If the abundance and scale length of disks evolves as indicated by Mao et al. (1998), then values of $p = 2$ and $q = -1$ are required if M^* evolves; values of $p = 3$ and $q = -2$ are required if M^* does not evolve.

Several physical processes can be invoked to explain the evolution of disks. If disks grow by the accretion of baryons from their halos, then the disk-to-halo mass ratio would be expected to be smaller at large redshifts. Disk–disk or disk–halo mergers would generally disrupt disks, reducing the abundance of disks at low redshifts. Low-mass disks could also be disrupted by supernova driven winds associated with episodes of powerful star formation. A determination of the evolution of the properties of disks would thus have important consequences for understanding the formation and evolution of galaxies.

The dominant contribution to the lensing cross section is provided by galaxies at redshifts less than unity. Hence, the results of Lilly et al. (1998), which sample this redshift range, should provide useful information about the normalization constant f_0 . In the absence of selection effects, the fraction of disks,

$$R_d \simeq \frac{\int_0^1 f_0(1+z')^p \frac{D(0, z')^2}{(1+z')^2} M^*(z') \frac{dr}{dz'} dz'}{\int_0^1 [1 - f_0(1+z')^p] \frac{D(0, z')^2}{(1+z')^2} M^*(z') \frac{dr}{dz'} dz'}, \quad (30)$$

subject to the constraint that $f_0(1+z')^p \leq 1$. If $p = 0$, then $R_d (\simeq 0.18) = f_0/(1-f_0)$, and so $f_0 \simeq 0.15$. If the disk fraction increases with increasing redshift, that is $p > 0$, then the value of f_0 will be reduced. The form of evolution of M^* has very little effect on the results. For values of $p = -1, 0, 1, 2$ and 3 , f_0 takes the values of $0.25, 0.15, 0.089, 0.051$ and 0.025 respectively.

Table 2. The values of the parameters in the disk lensing models used to derive the results in Figs 4 and 5. Both models are constrained by requiring that they provide a reasonable, if schematic, account of the abundance of disks determined in the CFRS fields by Lilly et al. (1998), normalized to the disk fraction at zero redshift found by Marzke (1998). In both models, disks have the same properties at all redshifts less than unity (Lilly et al. 1998). See Section 2.3.1 for a definition of the parameters f_0 , p and q .

Model	M^* evolution?	f_0	p	q
A	No	0.60	0	0
B	Yes	0.60	-1	1

In the absence of universal agreement on the interpretation of the CFRS data, we present forms of the functions a_1 , a_2 and a_3 derived for a range of different values of p and q to illustrate the possible effects of different forms of disk evolution: see Fig. 3. The most significant effects are produced by large values of q . These values correspond to models in which the disk to halo mass ratio evolves strongly. Large lens surveys carried out in the radio and millimetre/submillimetre wavebands should eventually provide a large sample of mass-selected lensed objects. These samples could be used to resolve any remaining uncertainty in the interpretation of existing surveys.

3.2 Forms of F_{disk} derived for evolving disks

The optical depths to strong lensing F_{disk} and F_{SIS} can now be calculated and compared. In Fig. 4 $F_{\text{disk}}/F_{\text{SIS}}$ is shown for both models of disk evolution listed in Table 2 as a function of both magnification and redshift. The optical depth to strong lensing is increased by incorporating the effect of lensing by disks by a factor between 2 and 3 at redshifts of about unity and magnifications of several tens. The effect of including disks is more significant at greater magnifications. The consequences for the counts of lensed galaxies and quasars in the submillimetre waveband are discussed below.

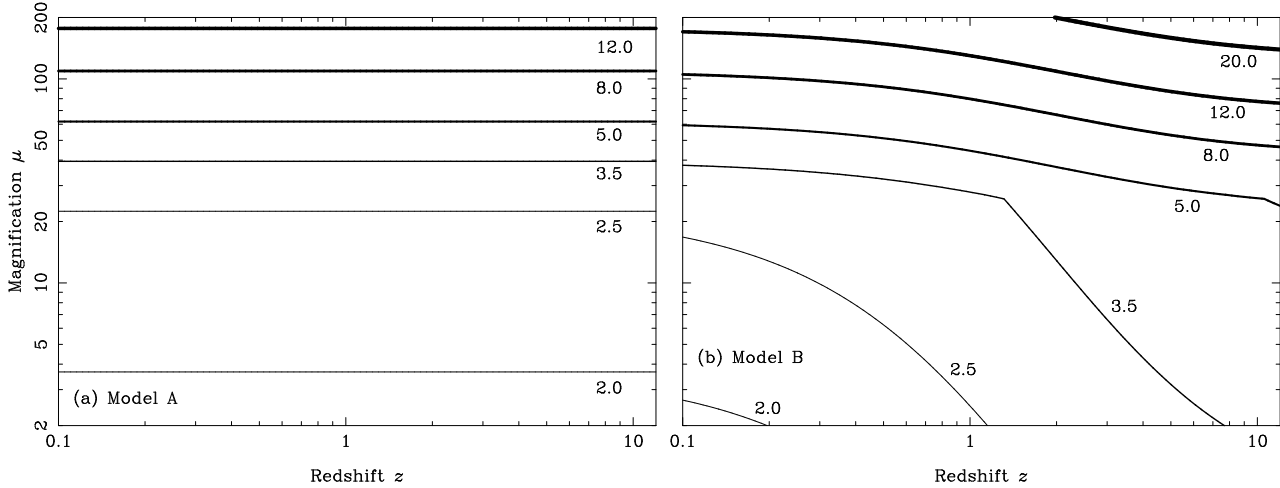


Figure 4. The ratio of the differential optical depths to high-magnification lensing produced by a population of disks within SIS halos and a population of pure SIS halos, $F_{\text{disk}}/F_{\text{SIS}}$ as a function of redshift and magnification. Models A and B, which include different values of the parameters p and q are defined in Table 2. The lensing parameters listed in Table 1 are assumed. The results are not affected significantly by changes to the world model.

4 LENSED GALAXIES IN THE SUBMILLIMETRE WAVEBAND

4.1 Introduction

The selection functions in submillimetre-wave surveys are very broad and extend out to high redshifts. This is because the flux density-redshift relation for distant dusty galaxies is expected to be flat over the range of redshifts from about 0.5 to 10, owing to large negative K -corrections. These arise when dust emission spectra, peaking in the rest-frame far-infrared waveband, are redshifted into the submillimetre waveband (Blain & Longair 1993). A submillimetre-wave survey thus selects high-redshift galaxies preferentially, and because a flat flux density-redshift relation naturally corresponds to a steep source count, magnification biases in such a survey are expected to be large (Blain 1996). At that time, however, source counts of submillimetre-wave sources had not been determined. Now Smail et al. (1997) have detected a population of distant dusty galaxies, including a dust-shrouded starburst/AGN at a redshift $z = 2.803$ (Ivison et al. 1998; Frayer et al. 1998). A fuller description of the survey (Smail et al. 1998, 1999, in preparation; Blain et al. submitted) and its consequences (Blain 1998c; Blain et al. 1998a, 1998b, 1999) can be found elsewhere. The results of other submillimetre-wave surveys are now becoming available (Barger et al. 1998; Eales et al. 1998; Holland et al. 1998; Hughes et al. 1998).

The surface density of galaxies with flux densities greater than 4 mJy at a wavelength of $850\text{ }\mu\text{m}$ is $(2.5 \pm 1.4) \times 10^3 \text{ deg}^{-2}$ (Smail et al. 1997). Counts of lensed galaxies that are consistent with these observations, which do not include the effects of lensing by disks, were presented by Blain (1998a,b,c). The local population of *IRAS* galaxies (Saunders et al. 1990) appears to undergo pure luminosity evolution of the form $(1+z)^\gamma$ where $\gamma \simeq 4$ out to $z \simeq 2.5$ (Blain et al. 1998c). This model is consistent with counts at other wavelengths in the millimetre/submillimetre waveband (Wilner & Wright 1997; Kawara et al. 1998; Lagache et al. 1998), and with the intensity of diffuse background radiation in the submillimetre/far-infrared waveband (Puget

et al. 1996; Guiderdoni et al. 1997; Schlegel, Finkbeiner & Davis 1998; Hauser et al. 1998; Fixsen et al. 1998).

4.2 Calculating counts of lensed galaxies

We determine counts of lensed galaxies by using equation (3) with Φ' calculated using F_{disk} (equation 15), normalised as described above, in both models of disk evolution described in Table 2. The population of distant dusty galaxies assumed is described by the ‘Gaussian’ model of Blain et al. (1999), which accounts for all the available submillimetre-wave and far-infrared data currently available.

In order to illustrate the expected form of the counts of both lensed and unlensed galaxies at wavelengths of 1300 , 850 , 450 and $60\text{ }\mu\text{m}$, the counts of galaxies expected in the absence of disks are compared in Fig. 5(a). Lensed counts are calculated, assuming that M^* does and does not evolve. If M^* does not evolve, then the predicted count of lensed galaxies is greater. As a result, all previous predictions have been made assuming that M^* evolves to produce conservative estimates of the counts of lenses. To demonstrate the effects of including lensing by disks, the relative size of the counts of lensed galaxies with disks as compared with the counts shown in Fig. 5(a) are shown in Fig. 5(b). The additional bias due to disk lensing is typically a factor of 2 and 3 in models A and B respectively.

The only data currently available on the population of lensed dusty galaxies and quasars is provided by the identification of two luminous distant $60\text{-}\mu\text{m}$ *IRAS* sources as lenses (Close et al. 1995; Irwin et al. 1998; Lewis et al. 1998), and the identification of one known lensed quasar with a $60\text{-}\mu\text{m}$ *IRAS* source (Kneib et al. 1998). This indicates a $60\text{-}\mu\text{m}$ count of at least $7 \times 10^{-5} \text{ deg}^{-2}$ lenses at a flux density of 0.2 Jy , fully consistent with the value of about $7 \times 10^{-4} \text{ deg}^{-2}$ shown in Fig. 5(a).

The maximum magnification assumed in these calculations for a source at $z = 1$, $\mu_{\text{max}}(1) = 40$, as assumed by Blain (1996). A larger value of μ_{max} will lead to a more significant effect of lensing by disks, as disks are progressively more efficient at producing large magnifications as compared

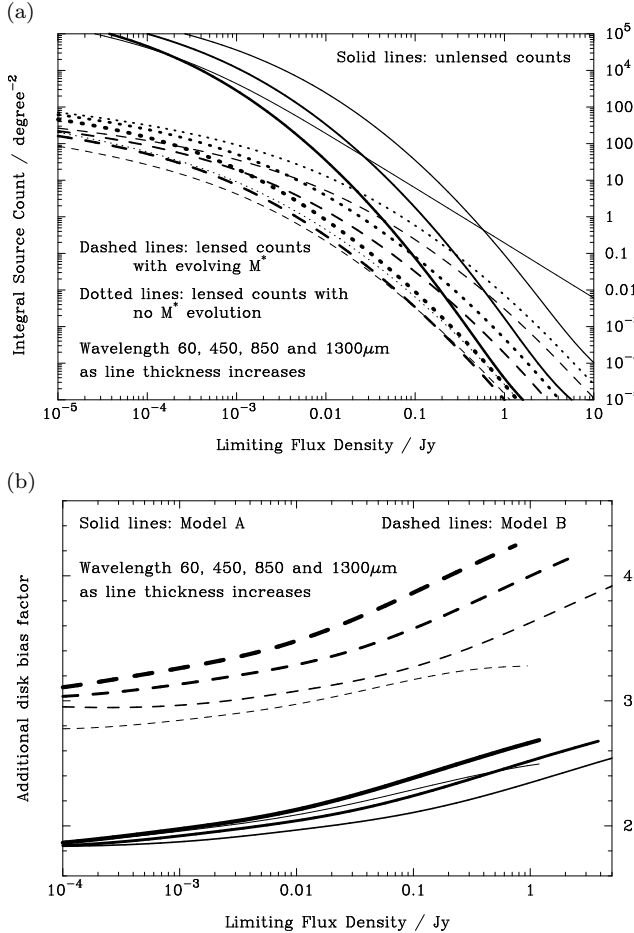


Figure 5. (a) Counts of lensed galaxies expected in the millimetre/submillimetre and far-infrared wavebands (Blain et al. 1998c). No effects of lensing by disks are included. Lensed counts with and without an evolving population of halos, as parametrized by M^* are shown. (b) The additional magnification bias factor that should multiply the counts in (a) when lensing by disks is considered in both models of disk evolution (Table 2 and Fig. 4). Some curves stop before the right-hand edge of the figures because the predicted counts fall below $2.4 \times 10^{-5} \text{ deg}^{-2}$ ($1/4\pi \text{ sr}^{-1}$).

with SIS halos: see Figs 1(a) and 4. This effect is emphasized in Fig. 6, in which the additional magnification bias due to lensing by disks is compared for different values of $\mu_{\max}(1)$: 10, 20, 40 and 100. Observations made using millimetre-wave interferometers (Solomon et al. 1997; Mirabel et al. 1998; Sakamoto et al. in press) indicate that the most luminous far-infrared emitting regions of distant galaxies are rather small, with scales of less than several hundred parsecs. As $\mu_{\max}(1) \simeq 25$ is expected for a 1-kpc source (Peacock 1982), $\mu_{\max}(1) = 40$ seems to be very reasonable. Larger magnifications may also be possible, at least for any very compact subsample of distant submillimetre-luminous galaxies and quasars, such as the ‘extreme starbursts’ imaged by Downes & Solomon (1998). In this case, the numbers of lenses with flux densities of order 100 mJy, and thus the magnification biases due to disks (Fig. 5b), will be increased.

The fraction of lensed galaxies detected in a carefully designed flux-limited submillimetre-wave survey is expected to be several per cent (Blain 1996, 1998b), and it is reason-

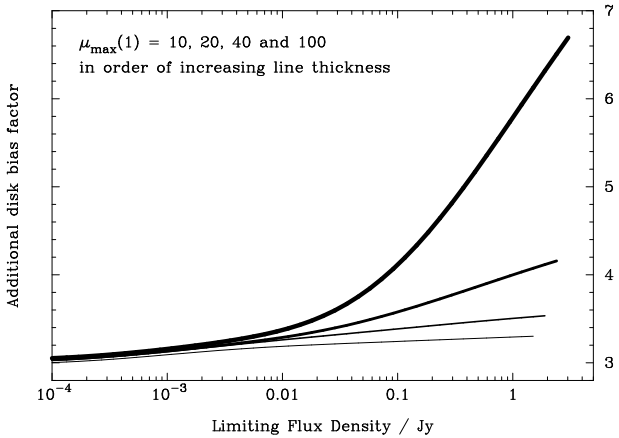


Figure 6. Differences in the additional magnification bias due to lensing by disks, expected at a wavelength of 850 μm in disk evolution Model B: see Table 2. A larger value of μ_{\max} corresponds to a more significant effect, emphasizing the results shown in Fig. 4.

able to expect lensing by disks to increase this fraction by a factor of between 2 and 3.

5 THE PROSPECTS FOR FUTURE OBSERVATIONS

5.1 Potential instruments

Many forthcoming instruments will be useful for carrying out submillimetre-wave lens surveys. Foremost amongst them are large ground-based millimetre/submillimetre interferometer arrays, such as the MMA (Brown 1996): see also Downes (1996) and Ishiguro et al. (1992). These instruments, with sub-arcsecond angular resolution, will be required in order to confirm submillimetre-selected lens candidates (Blain 1998b). Large single-antenna telescopes such as the US–Mexican 50-m Large Millimeter Telescope (LTM/GTM; Schloerb 1998) and a 10-m telescope at the South Pole (Stark et al. 1998), are also being designed and built. These telescopes will provide large and uniform focal planes, able to exploit large format bolometer array receivers (Glenn et al. 1998), and would be very useful for wide-field millimetre/submillimetre-wave surveys (Blain 1998c). The *Planck Surveyor* (Bersanelli et al. 1996) and *Far-Infrared and Submillimetre Telescope* (FIRST; Pilbratt 1997) space missions also have great potential.

5.2 The detection rate of lenses

The relative speed of detecting lenses using the instruments discussed above is considered in more detail elsewhere (Blain 1998c). There is freedom to choose a survey strategy for all but *Planck Surveyor*, and if optimized, detection rates of order 0.03–0.3 hour⁻¹ are expected. If the effect of lensing by disks is included, then these detection rates would be expected to increase by a factor of about 2 or 3. If the optical depth to submillimetre-wave lensing by disks is as large as we expect, then follow-up observations of detected lenses should reveal that a large fraction are lensed by edge-on disks. Submillimetre-wave point sources will be extracted from the

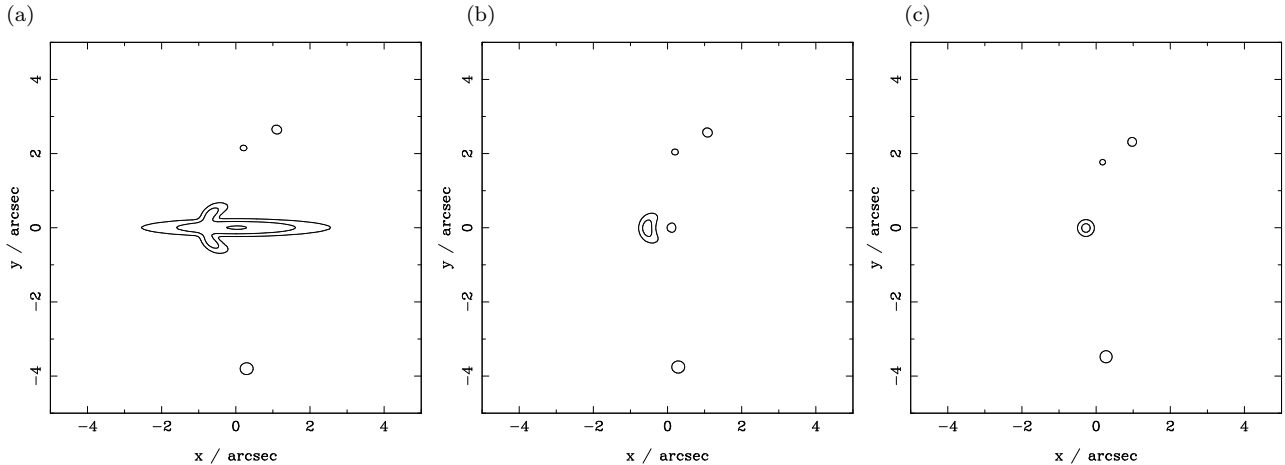


Figure 7. Simulated MMA images obtained at a wavelength of 850 mm for a representative region of sky that is chosen to contain a strongly lensed source. About 2 per cent of fields centred on a foreground galaxy would be expected to contain such a background source. The lensed images produced by a Milky Way galaxy at $z = 0.3$, inclined 5 degrees from the edge-on aspect, and the emission from the disk are shown in (a). In (b) the corresponding images produced by a SIS lens with the same mass as the disk, also at $z = 0.3$ are compared. The background population of sources are shown in (c). The contour levels correspond to the 1σ noise levels expected in 1-minute, 1-hour and 24-hour integrations: 220, 28 and $5.8 \mu\text{Jy beam}^{-1}$ respectively.

all-sky *Planck Surveyor* survey (Blain 1998b), down to the confusion limit (Blain et al. 1998a,b). More than a thousand lensed galaxies and quasars were predicted, without considering the effects of lensing disks. This number should also be increased by a factor of 2 or 3 when lensing by disks is taken into account.

5.3 Imaging lens candidates using the MMA

Multiple lensed images formed by galaxies are separated on arcsecond scales. A large interferometer array, such as the MMA, would thus be the ideal telescope with which to investigate lensing by distant galaxies in detail. In Fig. 7 we show simulated images of a 10-arcsecond wide field, contained within the primary beam of the MMA, at an angular resolution of 0.1 arcsec. The contour levels correspond to three times the $850\text{-}\mu\text{m}$ 1σ sensitivity limits in MMA integrations lasting 1 minute, 1 hour and 1 day: 220, 28 and $5.8 \mu\text{Jy beam}^{-1}$ respectively. Note that the primary beam area of the MMA at $850\text{-}\mu\text{m}$ is about $3 \times 10^{-5} \text{ deg}^{-2}$, and so the brightest source in this area would be expected to have a flux density of $40 \mu\text{Jy}$ (Fig. 5a). In Fig. 7(c) a typical region of the background sky is shown. The source distribution in this case is chosen so that one source will be magnified significantly by a disk galaxy at the centre of the figure. All sources are Gaussian and 0.2-arcsec across at full width half maximum. An alignment between source and lens this close or closer is expected in about 2 per cent of cases. In Fig. 7(a) the effects of lensing these sources by an edge-on disk galaxy, similar to the Milky Way, at a redshift of 0.3 is shown. The submillimetre-wave emission from the lensing galaxy is calculated by transforming the observation of a nearby edge-on disk galaxy (Israel, van der Werf & Tilanus 1998) to $z = 0.3$, giving a total flux density of about 1 mJy and a scale length of 1 arcsec. In Fig. 7(b) the much less significant effects of lensing by a SIS dark matter halo with the same mass at the same redshift are compared.

In addition to following up the sources detected in sur-

veys using single-antenna telescopes (Blain 1998c), a deep targeted MIA survey of known distant edge-on disks, provided for example by the Sloan Digital Sky Survey catalogue (Margon 1998), would be a very powerful way of detecting lensed images of very faint distant submillimetre-wave galaxies. Integration times of about 24 hours per source would be required however.

6 CONCLUSIONS

(i) We have estimated the enhanced magnification bias expected for statistical lensing due to a population of baryonic disks in dark matter halos. The bias is expected to be enhanced by a factor of 2 or 3 as compared with a population of SIS lenses. This bias could be much larger if the sources are smaller than several hundred parsecs in size, and can thus be magnified by a factor in excess of 40.

(ii) In the submillimetre waveband, lensed images will not suffer from the effects of dust absorption in the lensing galaxy. Hence images lensed by edge-on disks should be selected in an unbiased manner in submillimetre-wave surveys made using the MMA, LMT/GTM, a 10-m telescope at the South Pole, and the space-borne instruments *Planck Surveyor* and *FIRST*.

(iii) The subarcsecond angular resolution of the MMA will be required in order to study lensed images in detail. A targeted search of known edge-on disks could provide a fruitful technique for detecting and observing any very faint, distant dusty galaxies.

ACKNOWLEDGEMENTS

We thank Jarle Brinchmann, Malcolm Longair, Priya Natarajan, Joel Primack for helpful comments on the manuscript, the referee for his/her prompt reading of the manuscript and the Rotary Club of Erice for their hospitality. Observations made by Ian Smail, Rob Ivison, Jean-Paul

Kneib and AWB have assisted greatly in refining the conclusions of this paper.

REFERENCES

Barger A. J., Cowie L. L., Sanders D. B., Fulton E., Taniguchi Y., Sato Y., Kawara K., Okuda H., 1998, *Nat*, 394, 248

Bartelmann M., Loeb A., 1998, *ApJ*, 503, 48

Bersanelli M. et al., 1996, COBRAS/SAMBA. SCI(96)3, ESA publications, Paris

Blain A. W., 1996, *MNRAS*, 283, 1340

Blain A. W., 1997a, *MNRAS*, 290, 553

Blain A. W., 1997b, in Wilson A. ed., The Far-infrared and Submillimetre Universe. ESA SP-401, ESA publications, Noordwijk, p. 175 (astro-ph/9710139)

Blain A. W., 1998a, *MNRAS*, 295, 92 (astro-ph/9710160)

Blain A. W., 1998b, *MNRAS*, 297, 511 (astro-ph/9801098)

Blain A. W., 1998c, in Colombi S., Mellier Y. eds, Wide-field surveys in cosmology. Proceedings XIV IAP Meeting, Edition Frontières, Gif-sur-Yvette, in press (astro-ph/9806369)

Blain A. W., Longair M. S., 1993, *MNRAS*, 264, 509

Blain A. W., Ivison R. J., Smail I., 1998a, *MNRAS*, 296, L29 (astro-ph/9810003)

Blain A. W., Ivison R. J., Smail I., Kneib J.-P., 1998b, in Colombi S., Mellier Y. eds, Wide-field surveys in cosmology. Proceedings XIV IAP Meeting, Edition Frontières, Gif-sur-Yvette, in press (astro-ph/9806063)

Blain A. W., Smail I., Ivison R. J., Kneib J.-P., 1999, *MNRAS*, in press (astro-ph/9806062)

Blain A. W., Kneib J.-P., Ivison R. J., Smail I., ApJL, submitted

Brinchmann J., 1998, private communication

Brown R. L., 1996, in Bremer M. N., van der Werf P., Röttgering H. J. A., Carilli C. R. eds, Cold Gas at High Redshift. Kluwer, Dordrecht, p. 411

Browne I. W. A. et al., 1997, in Bremer M., Jackson N., Perez-Fournon I. eds., Observational Cosmology with the New Radio Surveys, Kluwer, Dordrecht, p. 305

Close L. M., Hall P. B., Liu C. T., Hege E. K., 1995, *ApJ*, 452, L9

Downes D., 1996, in Shaver P. ed., Science with Large Millimetre Arrays, Springer, Berlin, p. 16

Downes D., Solomon P. M., 1998, *ApJ*, in press (astro-ph/9806377)

Eales S. A., Lilly S. J., Gear W., Dunne L., Bond J. R., Hammer F., Le Févre O., Crampton D., 1998, *ApJL*, submitted (astro-ph/9808040)

Fixsen D. J., Dwek E., Mather J. C., Bennett C. L., Shafer R. A., 1998, *ApJ*, in press (astro-ph/9803021)

Frayer D. T., Ivison R. J., Scoville N. Z., Yun M. S., Evans A. S., Smail I., Blain A. W., Kneib J.-P., 1998, *ApJ*, 505, L7 (astro-ph/9808109)

Glenn J. et al., 1998, in Phillips T. G. ed., Advanced Technology MMW, Radio and Terahertz telescopes. Proc. SPIE vol. 3357, SPIE, Bellingham, in press

Guiderdoni B., Bouchet F. R., Puget J.-L., Lagache G., Hivon E., 1997, *Nat*, 390, 257

Hauser M. G. et al., 1998, *ApJ*, in press (astro-ph/9806167)

Holland W. S. et al. 1999, *MNRAS*, in press (astro-ph/9809122)

Holland W. S. et al., 1998, *Nat*, 392, 788

Hudson M. J., Gwyn S. D. J., Dahle H., Kaiser N., 1998, *ApJ*, 503, 529

Hughes D. H. et al., 1998, *Nat*, 394, 241

Irwin M. J., Ibata R. A., Lewis G. F., Totten E. J., *ApJ*, 505, 529

Ishiguro M., Kawabe R., Nakai N., Morita K.-I., Okumura S. K., Ohashi N., 1992, in Ishiguro M., Welch W. J. eds, Astronomy with millimeter and submillimeter interferometry, PASP conference series, vol. 59, p. 405

Israel F. P., van der Werf P. P., Tilanus R. P. J., 1998, *A&A*, in press (astro-ph/9806271)

Ivison R. J., Smail I., Le Borgne J.-F., Blain A. W., Kneib J.-P., Bézecourt J., Kerr T. H., Davies J. K., 1998, *MNRAS*, 298, 583 (astro-ph/9712161)

Kawara K. et al., 1998, *A&A*, 336, L9

Keeton C. R., Kochanek C. S., 1998, *ApJ*, 495, 157

Kneib J.-P., Alloin D., Mellier Y., Guilloteau S., Barvainis R., Antonucci R., 1998, *A&A*, 329, 827

Koopmans L. V. E., de Bruyn A. G., Jackson N., 1998, *MNRAS*, 295, 534

Lagache G. et al., 1998 in Colombi S., Mellier Y. eds, Wide-field surveys in cosmology. Proceedings XIV IAP Meeting, Edition Frontières, Gif-sur-Yvette, in press

Lewis G. F., Chapman S. C., Ibata R. A., Irwin M. J., Totten E. J., 1998, *ApJ*, 505, L1

Lilly S. J. et al., 1998, *ApJ*, 500, 75

Maller A. H., Flores R. A., Primack J. R., 1997, *ApJ*, 486, 681 (astro-ph/9701110)

Mao S., Mo H. J., White S. D. M., 1998, *MNRAS*, 297, L71

Margon B., 1998, *Phil. Trans. Roy. Soc. London*, in press (astro-ph/9805314)

Marzke R. O., da Costa L. N., Pellegrini P. S., Willmer C. N. A., Geller M. J., 1998, *ApJ*, 503, 617

Mirabel I. F. et al., 1998, *A&A*, 333, L1

Mo H. J., Mao S., White S. D. M., 1998, *MNRAS*, 295, 317

Möller O., 1996, MSci dissertation, University of Cambridge

Möller O., Blain A. W., 1998, *MNRAS*, 299, 845 (astro-ph/9806067)

Peacock J. A., 1982, *MNRAS*, 199, 987

Pei Y. C., 1995, *ApJ*, 440, 485

Pilbratt G., 1997, in Wilson A. ed., The Far-infrared and Submillimetre Universe. ESA SP-401, ESA publications, Noordwijk, p. 7

Press W. H., Schechter P., 1974, *ApJ*, 187, 425

Puget J.-L., Abergel A., Bernard J.-P., Boulanger F., Burton W. B., Désert F.-X., Hartmann D., 1996, *A&A*, 308, L5

Sakamoto K., Scoville N. Z., Yun M. S., Crosas M., Genzel R., Tacconi L. J., 1998, *ApJ*, in press (astro-ph/9810325)

Saunders W., Rowan-Robinson M., Lawrence A., Efstathiou G., Kaiser N., Ellis R. S., Frenk C. S., 1990, *MNRAS*, 242, 318

Schlegel D. J., Finkbeiner D. P., Davis M., 1998, *ApJ*, 500, 525

Schneider P., Ehlers J., Falco E. E., 1992, Gravitational lenses, Springer, Berlin

Schloerb F. P., 1997, in Latter W. B., Radford S. J. E., Jewell P. R., Mangum J. G., Bally J. eds, 25 years of millimeter spectroscopy. Proc. IAU 170, Kluwer, Dordrecht, p. 221

Smail I., Ivison R. J., Blain A. W., 1997, *ApJ*, 490, L5 (astro-ph/9708135)

Smail I., Ivison R. J., Blain A. W., Kneib J.-P., 1998, *ApJ*, 507, L21 (astro-ph/9806061)

Smail I., Ivison R. J., Blain A. W., Kneib J.-P., 1999, in Holt S. S., Smith E. P. eds, After the dark ages: when galaxies were young. AIP, Woodbury NY, in press (astro-ph/9810281)

Smail I. et al., in preparation

Solomon P. M., Downes D., Radford S. J. E., Barrett J. W., 1997, *ApJ*, 478, 144

Stark A. A., Carlstrom J. E., Israel F. P., Menten K. M., Peterson J. B., Phillips T. G., Sironi G., Walker W. W., 1998, in Phillips T. G. ed., Advanced Technology MMW, Radio and Terahertz telescopes. Proc. SPIE vol. 3357, SPIE, Bellingham, in press (astro-ph/9802326)

Wang Y., Turner E. L., 1997, *MNRAS*, 292, 863

Wilner D. J., Wright M. C. H., 1997, *ApJ*, 488, L67